JOURNAL OF
SYNCHROTRON
RADIATION

ISSN 1600-5775

Optimized spatial overlap in optical pump–X-ray probe experiments with high repetition rate using laser-induced surface distortions

Matthias Reinhardt,[a] Azize Koc,[a] Wolfram Leitenberger,[a] Peter Gaal[b]* and Matias Bargheer[a,c]

[a]Helmholtz-Zentrum Berlin für Materialien und Energie GmbH, Wilhelm-Conrad-Röntgen Campus, BESSY II, Albert-Einstein-Strasse 15, 12489 Berlin, Germany, [b]Institut für Nanostruktur- und Festkörperphysik, Universität Hamburg, Jungiusstrasse 11, 20355 Hamburg, Germany, and [c]Institut für Physik und Astronomie, Universität Potsdam, Karl-Liebknecht-Strasse 24–25, 14476 Potsdam, Germany. *Correspondence e-mail: pgaal@physnet.uni-hamburg.de

Received 10 September 2015
Accepted 18 December 2015

Edited by D. A. Reis, SLAC National Accelerator Laboratory, USA

Keywords: ultrafast X-ray diffraction; nanostructures; surface deformation; heat diffusion; optical pump.

Ultrafast X-ray diffraction experiments require careful adjustment of the spatial overlap between the optical excitation and the X-ray probe pulse. This is especially challenging at high laser repetition rates. Sample distortions caused by the large heat load on the sample and the relatively low optical energy per pulse lead to only tiny signal changes. In consequence, this results in small footprints of the optical excitation on the sample, which turns the adjustment of the overlap difficult. Here a method for reliable overlap adjustment based on reciprocal space mapping of a laser excited thin film is presented.

1. Introduction

Ultrafast X-ray diffraction (UXRD) offers the unique possibility to observe atomic and molecular motion in real time on femtosecond to picosecond timescales (Rousse & Gauthier, 2001; Bargheer *et al.*, 2006; Elsaesser & Woerner, 2014; Minitti *et al.*, 2015; Park *et al.*, 2015; Dufresne *et al.*, 2011). Owing to its wide range of applications UXRD has become an increasingly popular method. The high stability and high photon flux provided by synchrotron radiation at electron storage rings makes UXRD very sensitive to tiny lattice changes (Kozina *et al.*, 2014; Sheu *et al.*, 2008; Shayduk *et al.*, 2011). New X-ray sources such as free-electron lasers offer even better conditions, in particular a better temporal resolution, than third-generation synchrotron sources (Yabashi *et al.*, 2015; Chollet *et al.*, 2015). In a typical UXRD experiment a sample is excited with an ultrashort laser pulse. The sample response is captured with a short X-ray pulse with variable time delay with respect to the optical excitation pulse (Rose-Petruck *et al.*, 1999; Rousse & Gauthier, 2001; Navirian *et al.*, 2012). Optical excitation changes the phononic (Lee *et al.*, 2008), magnetic (Bigot & Vomir, 2013; Mariager *et al.*, 2012) or electronic (Schick *et al.*, 2014*a*) properties in the sample which in turn modify the crystal lattice. To exploit all useful photons in storage-ring-based facilities the repetition rate of the excitation lasers is increased up to the repetition rate of the X-ray pulses. A major difficulty is the increased thermal load on the sample, since the average pump power is the product of the optical pulse energy and the repetition frequency,

$$P_{\text{avg}} = E_{\text{pulse}} f_{\text{rep}}. \qquad (1)$$

According to (1), a low optical pulse energy of 10 µJ at a repetition frequency of 200 kHz results in an average power of 2 W on the sample. These parameters can lead to a discre-

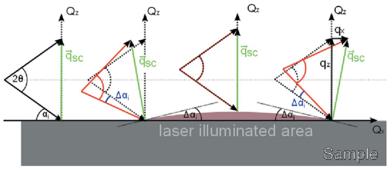

pancy between a transient temperature rise and an average sample heating due to the pump laser of up to 1:10 (Navirian *et al.*, 2012).

UXRD experiments are sensitive to transient changes of the lattice constant and are very sensitive to thermal distortions. The energy deposited by the pump pulse can cause surface deformations which may lead to a misinterpretation of the detected X-ray signal already at repetition rates of 1 kHz (Shymanovich *et al.*, 2007). In these experiments the diffraction angle and the diffracted intensity show a pronounced asymmetry with respect to scanning the pump laser across the probe spot. These effects are strongly enhanced at higher repetition rates where focusing of the excitation laser is used to maintain substantial pump intensities.

Here we specifically discuss problems and solutions for optimized spatial overlap of the pump and probe pulse which relies on a detailed study of the local lattice distortion induced by a laser spot focused on a sample.

2. Experimental method

Experiments were performed at the new XPP/KMC3 beamline at the synchrotron radiation source BESSY II. The XPP experimental station is dedicated to ultrafast X-ray diffraction (UXRD) and X-ray absorption experiments. Its layout is shown in Fig. 1(*a*). The energy spectrum extends from 2 keV to up to 16 keV in the hard X-ray region (Navirian *et al.*, 2012). Electron bunches orbit the storage ring with a frequency of 1.25 MHz. In addition to the customary hybrid filling pattern, the storage ring can be filled with a single electron bunch or operated in a low-charge mode, the so-called low-α mode, for higher temporal resolution (Holldack *et al.*, 2007; Kahn *et al.*, 2006).

At the XPP-KMC3 beamline (Fig. 1), the electrons accelerated by a bending magnet emit a beam of X-ray pulses which are collimated by a toroidal X-ray mirror (M1), monochromated by a double-crystal monochromator (MC) ($\Delta E/E = 10^{-4}$) and focused into the experimental hutch by a second toroidal mirror (M2). The focal length of M2 is 7 m which results in a vertical divergence of 0.52 mrad. The size of the X-ray beam at the focal point is 170 µm × 350 µm. A spherical aperture with a diameter of 50 µm can be introduced 5 cm before the focal point where the sample is positioned on a goniometer. The X-ray footprint on the sample is approximately 80 µm, according to the divergence.

We employ a commercial Yb-doped fiber laser (Impulse, Clark MXR) as a source for optical pump pulses. The laser delivers pulses with a duration of 260 fs and a pulse energy of 10 µJ at a wavelength of 1030 nm. The repetition rate can be varied between 200 kHz and 1.25 MHz. The laser is synchronized to the RF signal of the storage ring and the synchronization unit is employed as a time delay generator. Hence, the laser can be utilized as pump source for time-resolved optical pump–X-ray probe experiments (Navirian *et al.*, 2012).

As a compromise of sensitivity and heat load problems we typically choose 208 kHz repetition rate for pumping fully absorbing samples. Hence only every sixth X-ray camshaft pulse sees an optical pump pulse. Partially absorbing samples suffer less from the heat load and experiments can therefore be carried out at the full repetition rate of 1.25 MHz. Laser pulses are focused on the sample using a lens (L1) with a focal length of 750 mm. The lens is mounted on a set of motorized translation stages and can be positioned both perpendicular to and in the direction of the laser beam. The latter direction allows for changing the laser footprint on the sample, while the former allows for changing the position of the pump beam on the sample surface.

Diffracted X-rays are recorded by a two-dimensional hybrid pixel detector (Pilatus 100k, DECTRIS) (Henrich *et al.*, 2009). The detector allows for fast gating with a minimum duration of 70 ns which is sufficiently short for isolating the camshaft pulse in hybrid mode (Ejdrup *et al.*, 2009).

We exemplify the adjustment of the laser pump–X-ray probe overlap with a strontium ruthenate (SRO) thin film grown epitaxically on a strontium titanate (STO) substrate by pulsed laser deposition (Vrejoiu *et al.*, 2006). The metallic SRO layer has a thickness of 94 nm and an absorption length of 44 nm for an optical wavelength of 1030 nm (Korff Schmizing *et al.*, 2008; Kostic *et al.*, 1998). Hence, the excita-

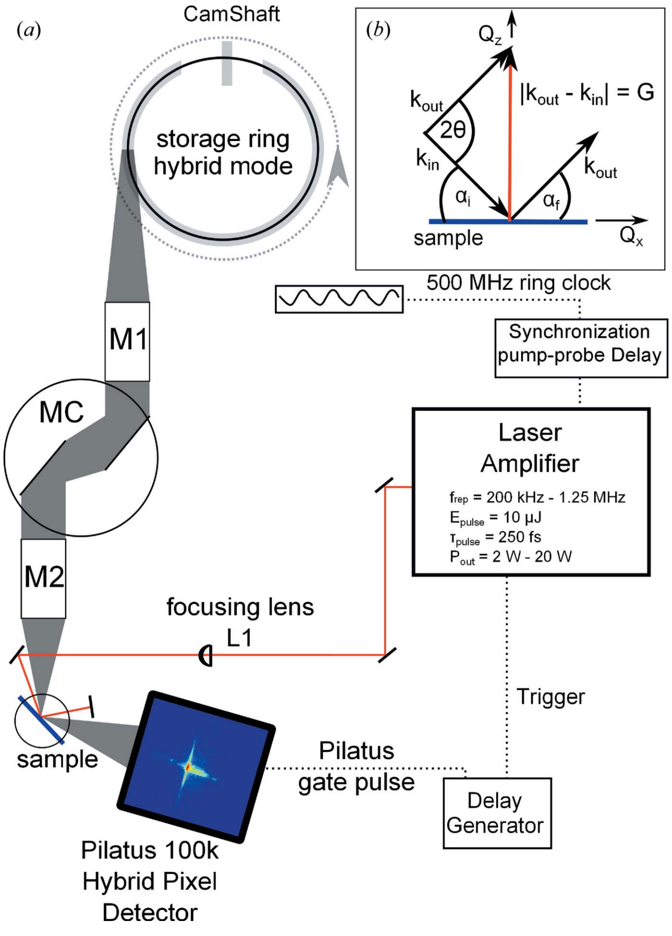

Figure 1
(*a*) Experimetal setup of the XPP/KMC3 beamline at BESSY II. (*b*) Diffraction geometry in reciprocal space from lattice planes parallel to the flat sample surface. The Q_x-direction is parallel and the Q_z-direction is normal to the sample surface.

tion pulses are fully absorbed in the thin film and lead to coherent strain waves on 100 ps timescale (Shayduk *et al.*, 2011) and thermal heat diffusion from the excited layer to the substrate on nanosecond to microsecond timescales (Navirian *et al.*, 2014; Schick *et al.*, 2014*b*).

3. Measuring the pump–probe overlap

In order to optimize the spatial overlap between pump and probe pulse, we record scattered X-ray photons from the (002) STO substrate reflection while scanning the optical excitation spot across the X-ray probe region. The diameter of the laser focus in the experiment was chosen to be approximately 400 µm. It is larger than the footprint of the X-ray probe beam on the sample, a basic requirement for pump–probe experiments. Absorption of the pump pulses in the SRO layer and subsequent thermal diffusion leads to a heating of the STO substrate and therefore to a thermal lattice expansion. The scanning of the probe region with the optical pulse is realised by the vertical (L_x) and horizontal (L_y) motion of L1. A vertical translation of L1 corresponds to a motion of the laser spot in the X-ray diffraction plane; a horizontal motion translates the laser spot in the direction perpendicular to the diffraction plane.

Even though our setup allows for measuring at the full temporal resolution of the synchrotron pulses of 100 ps (Shayduk *et al.*, 2013; Navirian *et al.*, 2014), we only present quasi-static measurements of the laser-excited sample in this contribution. However, spatial overlap is crucial for maximizing the transient response of a sample in a pump–probe experiment. With the two-dimensional detector it is possible to simultaneously detect specular and non-specular reflections from lattice planes, which are introduced by, for example, domain structures in a sample (Schick *et al.*, 2013*a*), by local strain fields due to dislocations or by thermal effects.

Fig. 2(*a*) shows a typical ω–2θ scan of the (002)-Bragg reflection of the SRO layer and STO substrate peaks, where $\omega = \alpha_{\rm i}$ and $2\theta = \alpha_{\rm i} + \alpha_{\rm f}$, as shown in Fig. 1(*b*). Fig. 2 presents experimental data for different alignment of the spatial overlap between optical pump and X-ray probe pulses.

The reciprocal lattice vector $\mathbf{q}_{002}$ of STO has been measured while scanning the exciting laser beam across the probe region. Diffracted X-rays were now detected with an area detector having a much larger surface than the X-ray footprint.[1]

First we neglect the spatial resolution of the area detector by integrating the detected X-ray photons across the whole detector surface. In this case the two-dimensional area detector is used as a point detector with a surface much larger than the X-ray beam size. The measured diffraction curves correspond to ω–2θ scans as shown in Fig. 2(*a*). However, the angular resolution of the detector position (2θ angle) is determined by the size of the detector area.

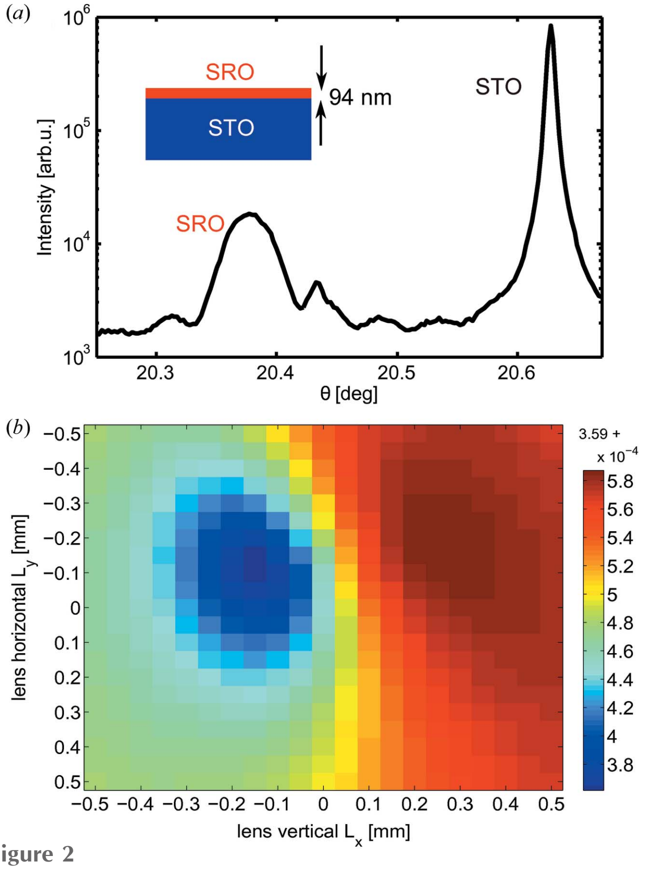

Figure 2
(*a*) ω–2θ scan of the (002) SRO layer and STO substrate Bragg reflection of an unexcited sample. The inset shows a sketch of the sample. (*b*) Center of the crystal truncation rod of the STO substrate in units of ang^{-1} at different horizontal and vertical alignments of the excitation laser.

In reciprocal space this scan corresponds to a scan along the crystal truncation rod (CTR). We denote this direction by the reciprocal space coordinate q_z. Fig. 2(*b*) shows the center of the CTR for different spatial overlap alignment. Blue regions denote smaller q_z values as expected for thermally expanded samples. Thus, Fig. 2(*b*) might suggest that the best spatial overlap between optical pump and X-ray probe pulse is obtained for vertical and horizontal lens positions of $L_{x,y}$ = (−0.15 mm, −0.1 mm). We will now show that this result is not correct by making use of the spatial resolution of the two-dimensional detector. The detector measures the diffracted intensity at different diffraction angles $\alpha_{\rm f}$. The measured diffracted intensity is mapped in reciprocal space using equation (2) (Schick *et al.*, 2013*b*; Holy *et al.*, 1999).

Figs. 3(*a*) and 3(*c*) show a decomposition of the scattered X-rays in a q_z- and q_x-component. The colorplots depict again a two-dimensional scan in $L_{x,y}$ of the excitation laser spot across the X-ray probe region on the sample. The minimum in the q_z-component is clearly visible at $L_{x,y}$ = (−0.05 mm, −0.15 mm) while q_x shows a zero-crossing from positive (red) to negative values (blue) at the same coordinate. The minimum in q_z is shifted by more than 100 µm compared with the minimum shown in Fig. 2(*b*). The characteristic features in q_z and q_x are highlighted by Figs. 3(*b*) and 3(*d*), showing cross sections at L_y = −0.15 mm of the q_z- and q_x-

---

[1] The X-ray spot covers one to four pixels of the detector; the translation during an angular scan of the footprint center of mass is of the order of the pixel size (172 µm × 172 µm).

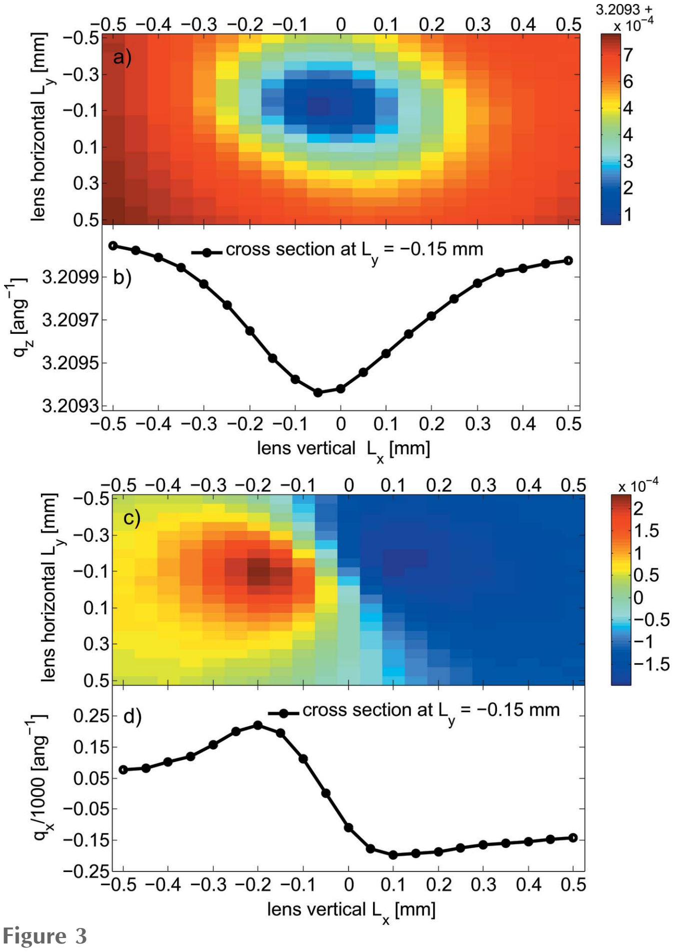

Figure 3
(a) The q_z-component of the (002) STO Bragg reflection *versus* vertical and horizontal lens position. (b) Cross section through (a) at a horizontal lens position of −0.15 mm. (c) The q_x-component of the same Bragg reflection *versus* vertical and horizontal lens position. (d) Cross section through (c) at a horizontal lens position of −0.15 mm.

component, respectively. In the minimum at $L_x = -0.15$ mm, q_z has a a value of 3.2094 Å^{-1}. At the same coordinates q_x becomes zero while crossing from a maximum at smaller vertical lens coordinates to a minimum at higher vertical lens coordinates.

Fig. 4 visualizes our interpretation of the data. Fig. 4(a) shows a simulation of the laser-induced thermal strain fields in the sample (Navirian *et al.*, 2012) resulting from the local deposition of heat at the surface. Absorption of the excitation laser in the sample leads to a significant heating and thus to a local expansion of the sample surface. The distortion, which is caused by the incident laser, can be scanned across the sample surface by translation of the focusing lens L1.

We distinguish different situations, that are visualized in Figs. 4(b)–4(e): in Fig. 4(b) the laser spot is far away from the probe region, which leaves the X-ray response more or less unaffected by laser heating. Hence, the diffraction geometry is purely symmetric and the scattering vector is oriented parallel to the Q_z-axis.

As soon as the laser approaches the probe area, the sample surface becomes distorted at the probe spot (Fig. 4c), which results in an asymmetric diffraction geometry. The scattering vector now has an additional component parallel to the Q_x-axis.

When the excitation laser overlaps with the probe area (Fig. 4d), the scattering vector is again oriented along the Q_z-axis. Here we assume that the excitation region is larger than the probe area, which is certainly the case in our measurement. The local heating of the probe area leads to an expansion of the crystal lattice and therefore to a decrease of the scattering vector $\mathbf{q}_{\rm sc}$ compared with Fig. 4(b). In addition, $\mathbf{q}_{\rm sc}$ is again parallel to the CTR, *i.e.* $\mathbf{q}_x = 0$.

Finally, translating the laser spot further (Fig. 4e) results again in a tilted diffraction geometry introduced by the surface distortion due to the local heating by the excitation laser. Since the slope of the surface tilt is now reversed in comparison with the case shown in Fig. 4(c), the x-component of the scattering vector points in the opposite direction.

In summary, the best overlap can be recognized for scattered wavevectors $\mathbf{q}_{\rm sc}$ having a minimal $\mathbf{q}_z$- and a vanishing $\mathbf{q}_x$-component. This situation is depicted in Fig. 4(d).

For alignment of the spatial overlap it is not necessary to measure complete maps as shown in Fig. 3. Each data point in the map represents a complete ω-scan of the sample. The duration of one scan is 20 s and the map contains 21 × 21 data points. Hence the measurement time for the whole map is 21 × 21 × 20 = 8820 s, which is almost 2.5 h. However, for aligning the spatial overlap it is sufficient to scan one line in the horizontal and vertical direction. The duration of the measurement then becomes 2 × 21 × 20 s = 14 min. This is a reasonable duration for a reliable alignment scan.

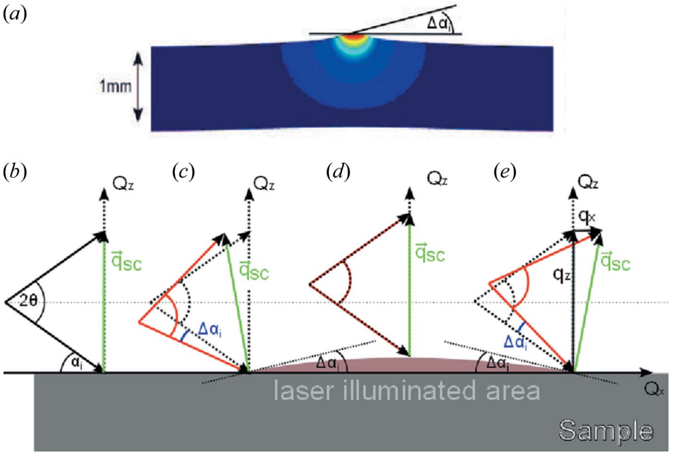

Figure 4
(a) Distortion of the sample surface due to the exciting optical pump beam. The simulation is taken from Navirian *et al.* (2012). (b) Scattering geometry of the unexcited sample. The scattering vector $\mathbf{q}_{\rm sc}$ is parallel to the Q_z-axis. (c) The rising slope of the near-surface distortion of the sample leads to a decrease of $\alpha_{\rm i}$. The scattering vector $\mathbf{q}_{\rm sc}$ is now composed of a positive q_z- and a negative q_x-component. (d) In the center of the excitation spot the sample is almost homogeneously excited in the lateral direction. The center of the CTR is shifted to smaller Q_z-values due to thermal expansion of the lattice. The scattering vector $\mathbf{q}_{\rm sc}$ is again parallel to the Q_z-axis, *i.e.* $q_x = 0$. (e) Similar to (c); however, the falling slope leads to an increased diffraction angle $\alpha_{\rm i}$. The scattering vector is now composed of a positive q_z and a positive q_x-component. The decomposition of the scattering vector $\mathbf{q}_{\rm sc}$ into a q_z- and a q_x-component is shown.

4. Surface profile

Fig. 4(*e*) visualizes the decomposition of the total scattered wavevector $\mathbf{q}_{\rm sc}$ into its components q_z and q_x along the reciprocal space directions Q_z and Q_x, respectively. The structure of the near-surface sample region can be extracted from the experimental data shown in Fig. 3 using the transformation (Schick *et al.*, 2013*b*; Holy *et al.*, 1999)

$$\mathbf{q} = \begin{pmatrix} q_x \\ q_z \end{pmatrix} = k \begin{bmatrix} \cos(\alpha_{\rm f}) - \cos(\alpha_{\rm i}) \\ \sin(\alpha_{\rm i}) + \sin(\alpha_{\rm f}) \end{bmatrix}, \qquad (2)$$

where $k = 2\pi/\lambda_{\rm xray}$ is the magnitude of the incident wavevector. The absolute reference angle ω for the STO substrate peak at an X-ray energy of 9 keV is 20.66°. In a symmetric geometry the incidence angle of X-rays to the surface is $\alpha_{\rm i} = \alpha_{\rm f} + \Delta\alpha_{\rm i}$, where $\Delta\alpha_{\rm i}$ is the near-surface tilt due to the laser heating. Evaluating equation (2) with the assumption $|\mathbf{q}| \approx q_z$ yields

$$\Delta\alpha_{\rm i} = \cos^{-1}\left[\cos(\alpha_{\rm f}) - \frac{q_x}{k}\right] - \alpha_{\rm f}. \qquad (3)$$

In our experiment we find $\Delta\alpha_{\rm i} = 0.011°$. Assuming a linear slope of the heat-induced surface expansion $\Delta h_{\rm surf}$, one finds

$$\Delta h_{\rm surf} = \frac{1}{2}\, d_{\rm ex} \tan(\Delta\alpha_{\rm i}), \qquad (4)$$

where $d_{\rm ex}$ is the size of the excitation footprint. For our measurement we find $h_{\rm surf} \approx 39$ nm with $d_{\rm ex} = 400$ µm at an average laser power of 1.2 W. In Fig. 5 we compare a spatial heat profile with a Gaussian shape, as produced by the Gaussian excitation pulse shape, with a linear approximation. The approximation introduces an error in the flat region on top of the Gaussian distribution. The Gaussian expansion profile and the linear approximation are shown by the black solid and blue dotted lines. The extrapolated linear heat profile overestimates the maximum temperature by roughly 15%.

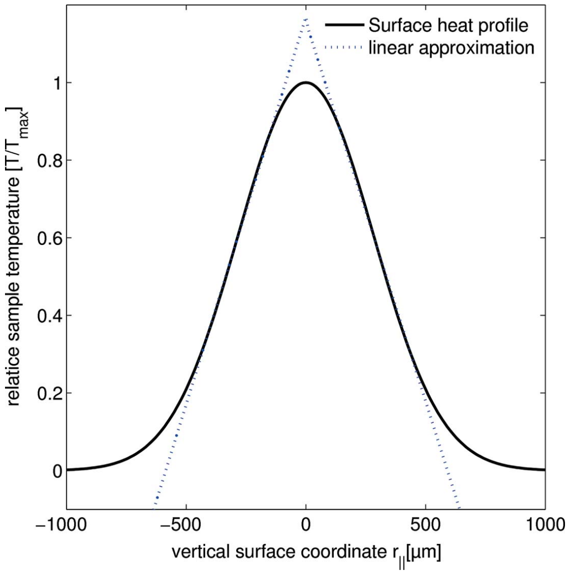

Figure 5
Linear approximation (blue dotted line) of the Gaussian thermal profile (black solid line) on the sample surface.

5. Conclusion

We propose a new method for optimizing the spatial alignment between optical pump and X-ray probe pulses in UXRD experiments. The method relies on the decomposition of the scattered X-ray wavevector into its in-plane and out-of-plane components. While our demonstration was performed in a quasi-static experiment, the method is of particular interest for time-resolved applications. The best spatial overlap position is recognized when the q_x-component vanishes while the q_z-component is minimized. Comparison with measurements that do not decompose the reciprocal lattice vector yield a different set of spatial coordinates for the overlap. Hence, a decomposition of the scattered wavevector into q_z- and q_x-components is essential. The surface distortion due to the inhomogeneous heating of the surface by the laser pulse can be reconstructed *via* the induced tilt of the reciprocal space vector in the q_x-direction. We demonstrate a nanometer sensitivity for surface distortions that result from the extreme pumping conditions in UXRD experiments, especially at high laser repetition rates.

Acknowledgements

We thank the BMBF for funding the project *via* 05K10IP1.

References

Bargheer, M., Zhavoronkov, N., Woerner, M. & Elsaesser, T. (2006). *ChemPhysChem*, **7**, 783–792.

Bigot, J.-Y. & Vomir, M. (2013). *Annal. Phys.* **525**, 2–30.

Chollet, M., Alonso-Mori, R., Cammarata, M., Damiani, D., Defever, J., Delor, J. T., Feng, Y., Glownia, J. M., Langton, J. B., Nelson, S., Ramsey, K., Robert, A., Sikorski, M., Song, S., Stefanescu, D., Srinivasan, V., Zhu, D., Lemke, H. T. & Fritz, D. M. (2015). *J. Synchrotron Rad.* **22**, 503–507.

Dufresne, E. M., Adams, B., Chollet, M., Harder, R., Li, Y., Wen, H., Leake, S. J., Beitra, L., Huang, X. & Robinson, I. K. (2011). *Nucl. Instrum. Methods Phys. Res. A*, **649**, 191–193.

Ejdrup, T., Lemke, H. T., Haldrup, K., Nielsen, T. N., Arms, D. A., Walko, D. A., Miceli, A., Landahl, E. C., Dufresne, E. M. & Nielsen, M. M. (2009). *J. Synchrotron Rad.* **16**, 387–390.

Elsaesser, T. & Woerner, M. (2014). *J. Chem. Phys.* **140**, 020901.

Henrich, B., Bergamaschi, A., Broennimann, C., Dinapoli, R., Eikenberry, E., Johnson, I., Kobas, M., Kraft, P., Mozzanica, A. & Schmitt, B. (2009). *Nucl. Instrum. Methods Phys. Res. A*, **607**, 247–249.

Holldack, K., Hartrott, M. v., Hoeft, F., Neitzke, O., Bauch, E. & Wahl, M. (2007). *Proc. SPIE*, **6771**, 677118.

Holy, V., Pietsch, U. & Baumbach, T. (1999). *High-Resolution X-ray Scattering from Thin Films and Multilayers, Springer Tracts in Modern Physics*, 1st ed. Berlin: Springer.

Khan, S., Holldack, K., Kachel, T., Mitzner, R. & Quast, T. (2006). *Phys. Rev. Lett.* **97**, 074801.

Korff Schmising, C. v., Harpoeth, A., Zhavoronkov, N., Ansari, Z., Aku-Leh, C., Woerner, M., Elsaesser, T., Bargheer, M., Schmidbauer, M., Vrejoiu, I., Hesse, D. & Alexe, M. (2008). *Phys. Rev. B*, **78**, 060404.

Kostic, P., Okada, Y., Collins, N. C., Schlesinger, Z., Reiner, J. W., Klein, L., Kapitulnik, A., Geballe, T. H. & Beasley, M. R. (1998). *Phys. Rev. Lett.* **81**, 2498–2501.

Kozina, M., Hu, T., Wittenberg, J. S., Szilagyi, E., Trigo, M., Miller, T. A., Uher, C., Damodaran, A., Martin, L., Mehta, A., Corbett, J., Safranek, J., Reis, D. A. & Lindenberg, A. M. (2014). *Struct. Dyn.* **1**, 034301.

Lee, H. J., Workman, J., Wark, J. S., Averitt, R. D., Taylor, A. J., Roberts, J., McCulloch, Q., Hof, D. E., Hur, N., Cheong, S.-W. & Funk, D. J. (2008). *Phys. Rev. B*, **77**, 132301.

Mariager, S. O., Pressacco, F., Ingold, G., Caviezel, A., Möhr-Vorobeva, E., Beaud, P., Johnson, S. L., Milne, C. J., Mancini, E., Moyerman, S., Fullerton, E. E., Feidenhans'l, R., Back, C. H. & Quitmann, C. (2012). *Phys. Rev. Lett.* **108**, 087201.

Minitti, M. P., Budarz, J. M., Kirrander, A., Robinson, J. S., Ratner, D., Lane, T. J., Zhu, D., Glownia, J. M., Kozina, M., Lemke, H. T., Sikorski, M., Feng, Y., Nelson, S., Saita, K., Stankus, B., Northey, T., Hastings, J. B. & Weber, P. M. (2015). *Phys. Rev. Lett.* **114**, 255501.

Navirian, H. A., Schick, D., Gaal, P., Leitenberger, W., Shayduk, R. & Bargheer, M. (2014). *Appl. Phys. Lett.* **104**, 021906.

Navirian, H., Shayduk, R., Leitenberger, W., Goldshteyn, J., Gaal, P. & Bargheer, M. (2012). *Rev. Sci. Instrum.* **83**, 063303.

Park, J., Zhang, Q., Chen, P., Cosgriff, M. P., Tilka, J. A., Adamo, C., Schlom, D. G., Wen, H., Zhu, Y. & Evans, P. G. (2015). *Rev. Sci. Instrum.* **86**, 083904.

Rose-Petruck, C., Jimenez, R., Guo, T., Cavalleri, A., Siders, C. W., Rksi, F., Squier, J. A., Walker, B. C., Wilson, K. R. & Barty, C. P. J. (1999). *Nature (London)*, **398**, 310–312.

Rousse, A., Rischel, C. & Gauthier, J.-C. (2001). *Rev. Mod. Phys.* **73**, 17–31.

Schick, D., Bojahr, A., Herzog, M., Gaal, P., Vrejoiu, I. & Bargheer, M. (2013*a*). *Phys. Rev. Lett.* **110**, 095502.

Schick, D., Herzog, M., Bojahr, A., Leitenberger, W., Hertwig, A., Shayduk, R. & Bargheer, M. (2014*b*). *Struct. Dyn.* **1**, 064501.

Schick, D., Herzog, M., Wen, H., Chen, P., Adamo, C., Gaal, P., Schlom, D. G., Evans, P. G., Li, Y. & Bargheer, M. (2014*a*). *Phys. Rev. Lett.* **112**, 097602.

Schick, D., Shayduk, R., Bojahr, A., Herzog, M., von Korff Schmising, C., Gaal, P. & Bargheer, M. (2013*b*). *J. Appl. Cryst.* **46**, 1372–1377.

Shayduk, R., Herzog, M., Bojahr, A., Schick, D., Gaal, P., Leitenberger, W., Navirian, H., Sander, M., Goldshteyn, J., Vrejoiu, I. & Bargheer, M. (2013). *Phys. Rev. B*, **87**, 184301.

Shayduk, R., Navirian, H. A., Leitenberger, W., Goldshteyn, J., Vrejoiu, I., Weinelt, M., Gaal, P., Herzog, M., Korff Schmising, C. v. & Bargheer, M. (2011). *New J. Phys.* **13**, 093032.

Sheu, Y. M., Lee, S. H., Wahlstrand, J. K., Walko, D. A., Landahl, E. C., Arms, D. A., Reason, M., Goldman, R. S. & Reis, D. A. (2008). *Phys. Rev. B*, **78**, 045317.

Shymanovich, U., Nicoul, M., Blums, J., Sokolowski-Tinten, K., Tarasevitch, A., Wietler, T., Horn von Hoegen, M. & von der Linde, D. (2007). *Appl. Phys. A*, **87**, 7–11.

Vrejoiu, I., Le Rhun, G., Pintilie, L., Hesse, D., Alexe, M. & Gösele, U. (2006). *Adv. Mater.* **18**, 1657–1661.

Yabashi, M., Tanaka, H. & Ishikawa, T. (2015). *J. Synchrotron Rad.* **22**, 477–484.